Process monitoring of chalcopyrite photovoltaic technologies by Raman spectroscopy: an application to low cost electrodeposition based processes

Victor Izquierdo-Roca,[a] Xavier Fontané,[b] Edgardo Saucedo,[b] Jesus Salvador Jaime-Ferrer,[c] Jacobo Álvarez-García,[d] Alejandro Pérez-Rodríguez,*[ab] Veronica Bermudez[c] and Joan Ramon Morante[ab]

Received (in Montpellier, France) 13th October 2010, Accepted 28th October 2010
DOI: 10.1039/c0nj00794c

This work describes the use and capabilities of Raman scattering for process monitoring and quality control applications in thin film chalcopyrite photovoltaic technologies. Main vibrational modes in the Raman spectra from the chalcopyrite layers are very sensitive to features related to their crystalline quality, chemical composition and the presence of secondary phases that are relevant for the optoelectronic properties of the absorbers and the efficiency of the solar cells and modules. Measurements performed at different process steps allow for the monitoring of the synthesis process of the chalcopyrite layers, giving information directly related to their processing conditions. These techniques have been successfully applied for the monitoring at on-line and *in situ* (real time) levels of the electrodeposition processes involved in the fabrication of low cost electrochemical based chalcopyrite solar cells. The results obtained corroborate the strong potential of Raman scattering for these applications, and open interesting perspectives on the development of new real time process control strategies.

Introduction

Thin film chalcopyrite technologies based on $CuInSe_2$ and its related alloys—such as $Cu(In,Ga)(S,Se)_2$—have received in the last few years a strong interest, because of their potential for the development of high efficiency low cost solar cells and modules. The efficiency of chalcopyrite based laboratory cells[1] has recently achieved a record value higher than 20%. The industrial implementation of these technologies at mass production levels has very low potential environmental impact, in spite of the acute toxicity of metals used in the synthesis of the layers, such as Cu. In this sense, leaching tests in the environment have shown that no real concern should be considered. This is related to the high stability of the compounds involved in the cells, as well as to the low amount of material required in the modules (about 1.8 g m^{-2}). To minimise these effects, module recovery plans are being already implemented almost for all industrial producers.

However, attaining high efficiency values in commercial modules is challenging due to the narrow process window existing in several steps of the production process. In particular, the performance of photovoltaic devices is highly sensitive to small fluctuations of the optoelectronic properties in the absorber layer. In terms of the production of large area modules, variations localised in small areas may result in the degradation of the overall performance of the device.

[a] *IN²UB, Departament d'Electrònica, Universitat de Barcelona, C. Martí i Franquès 1, 08028 Barcelona, Spain*
[b] *IREC—Catalonia Institute for Energy Research, C. Jardins de les Dones de Negre 1, 08930 Sant Adrià del Besòs (Barcelona), Spain. E-mail: aperezr@irec.cat*
[c] *NEXCIS, Zone Industrielle 190 Av. Celestin Coq, 13790 Rousset Cedex, France*
[d] *Centre de Recerca i Investigació de Catalunya (CRIC), Trav. de Gràcia 108, 08012 Barcelona, Spain*

The need for accurately controlled processing conditions in the production of chalcopyrite absorbers has led to the development of different non-destructive optical monitoring and quality assessment techniques, including optical reflectance, laser light scattering, ellipsometry, and Raman Spectroscopy (RS).[2] The successful implementation of these techniques would allow establishing rejection criteria at an early stage of the production process, thus avoiding the need to produce and test the complete module in case the absorber does not reach certain target characteristics. Considering the fact that the manufacture of the complete module usually involves several additional steps that together represent a significant fraction of the total production cost of the module, as well as the sensitivity of photovoltaic industry to cost issues, monitoring methods are becoming increasingly important.

RS has an enormous potential as a monitoring tool due to its ability to provide information on the chemical and structural properties of the films. RS is based on the spectroscopic analysis of the light inelastically scattered by a material. In a typical set-up, a monochromatic laser beam is focused onto the surface of the substrate under analysis, and the scattered light is collected and guided to a sensitive spectrometer. Inelastically light scattering occurs as a result of the interaction between the electric field associated to the incoming photons and the atomic polarizability of the crystal. As a result of this interaction, the scattering spectrum is characterised by a number of sharp bands, which are related to the energy of the zone-centre phonons in the crystal, and therefore, strongly depend on the chemical composition and crystallographic structure of the material.

In this work, the potential of using RS as a quality assessment and monitoring tool in the production of chalcopyrite absorbers is described, with a particular emphasis on the most

relevant structures: $CuInSe_2$ (CISe), $CuInS_2$ (CIS), $CuGaS_2$ (CGS) and $CuGaSe_2$ (CGSe). In the first part of the "Results and Discussion" section, the most important information that can be inferred from the analysis of the Raman spectra is discussed, including crystalline quality, crystallographic structure, chemical composition in the case of quaternary alloys, and the presence of secondary phases. The second part of this section deals with the experimental implementation of RS for monitoring of the electrodeposition step involved in the fabrication of electrochemical based $CuIn(S,Se)_2$ solar cells. Single step electrodeposition of $CuInSe_2$ precursors followed by a Rapid Thermal Process (RTP) sulfurisation has a strong interest for the development of technologies with low fabrication costs.[3,4] The results obtained on the characterisation of these processes corroborate the strong potential of RS in process monitoring applications, either as an on-line quality control tool or as an *in situ* technique for real time process monitoring.

Experimental

S-rich $CuIn(S,Se)_2$ absorbers with different composition (including stoichiometric $CuInS_2$) were grown on Mo coated glass substrates following a two step process, as described in ref. 3 and 4. In the first step, $CuInSe_2$ nanocrystalline precursors are grown on Mo-coated glass substrates with a single electrodeposition process in an acid bath containing Cu(II), In(III) and Se(IV) species. The thickness of these precursor layers is 1.6 μm, as estimated from cross section SEM pictures. In order to analyze the viability of Raman scattering measurements for the non-destructive monitoring of the precursor composition, the precursor layers were deposited with different values of the stoichiometry factor (m = 2Se/(Cu + 3In)) between 1.1. and 1.7, with a Cu/In content ratio between 1.1 and 1.2. At these conditions, the optimum range of values of stoichiometry is $1.3 \leq m \leq 1.4$. In the second step, the precursors are recrystallized under sulfurising conditions in a Rapid Thermal Process (RTP) at 650 °C. After the RTP process, the absorbers are treated in a 1 M NaCN bath in order to etch Cu(S,Se) secondary phases related to Cu excess segregation. Next steps for the fabrication of the cells are chemical bath deposition of a thin buffer CdS layer and RF-sputtering of the ZnO window layer.

In addition, polycrystalline $Cu(In,Ga)Se_2$ reference layers with different compositions (including stoichiometric $CuInSe_2$ and $CuGaSe_2$ layers) grown by the co-evaporation processes described in ref. 5 and 6, have also been analysed, to determine the dependence of the Raman spectra on the chemical composition of quaternary chalcopyrite alloys.

Ex situ Raman scattering measurements were performed on the processed layers using a T64000 Horiba Jobin-Yvon spectrometer, working in backscattering configuration. Excitation was provided with the 514.5 nm emission line from an Ar^+ laser. On the other hand, implementation of Raman scattering measurements for the *in situ* analysis of the electrodeposition process of the precursor layers has been performed using a portable fibre-coupled low-resolution equipment, potentially suitable for process monitoring applications at different environments. The Raman system (BWTEK) includes a single grating spectrometer (BTC-161-E) coupled to a compact immersion fibre optic probe, able to withstand the harsh acidic conditions in the electrolyte medium. The probe contains a band-pass filter to reject the Raman signal from the fibre, as well as a notch filter to minimise stray light in the spectrometer. A temperature stabilised solid state laser was used as the excitation source (wavelength 785 nm).

Results and discussion

Inelastic light scattering of chalcopyrite absorbers

Vibrational properties of chalcopyrite materials. The inelastic light scattering spectrum of chalcopyrite crystals is determined by the symmetry of the crystallographic space group ($I\bar{4}2d$), and by the presence of two molecular formulas (eight atoms) in each unit cell. As a result, chalcopyrite materials have 21 optical modes, which can be arranged according to their symmetry in the form of:

$$\Gamma_{opt} = A_1 \oplus 2A_2 \oplus 3B_1 \oplus 3B_2 \oplus 6E$$

All these vibrational modes—except those with A_2 symmetry—contribute to the Raman spectrum. However, the low scattering efficiency of these materials together with the fact that the frequency of many of these bands overlap often hinder the interpretation of the scattering spectra. Fortunately, A_1 symmetry modes give rise to a distinctive and intense peak in the scattering spectrum, which provides useful information on the characteristics of the material.

Fig. 1 shows the Raman spectra of three relevant chalcopyrite materials: $CuInSe_2$, $CuInS_2$ and $CuGaSe_2$. The spectrum from $CuGaS_2$ (not shown in this figure) is very similar, with a main A_1 mode centred at 310 cm^{-1}. In all cases, the spectra are characterised by a dominant peak arising from the interaction of light with the A_1 symmetry zone centre phonon. This vibrational mode involves the displacement only of the anions in the lattice in an anti-phase motion following the X–Y crystallographic directions of the crystal, while cations remain at rest.[7] This feature makes this band extremely sensitive to variations in the chemical and/or physical structure of the crystal, and supports the use of this band as a quality indicator in process monitoring applications.

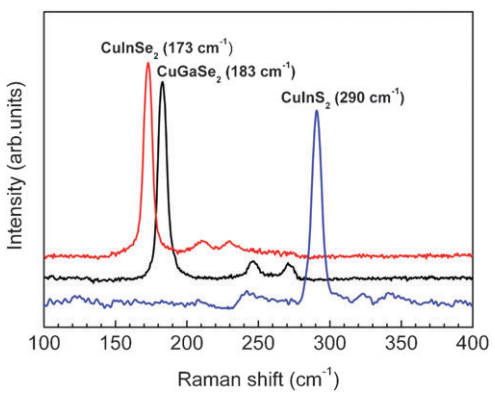

Fig. 1 Raman spectra from $CuInSe_2$, $CuInS_2$ and $CuGaS_2$. Spectra are normalised to the intensity of the dominant A_1 peak, and spectra from the different samples are vertically shifted.

In each particular compound, the vibrational frequency of the A_1 band is determined by the force constants of the cation–anion interaction, as well as by the anion mass (this mode does not involve cation displacements). Consequently, the frequency of the A_1 band in CISe is lower than in CIS, due to the higher mass of the Se atoms with respect to S ones. Likewise, the frequency of the A_1 band in CGS is higher than in CIS, since the bonding force constant of Ga–S is higher than that of In–S (the later with a larger atomic radius).

Assessment of crystalline quality in polycrystalline films. The Raman spectra of photovoltaic polycrystalline absorbers present relevant differences with respect to the reference spectra of defect-free single crystals. Such features may be exploited in process monitoring applications, enabling the evaluation of the crystalline quality of the films. In particular, the Full Width at Half Maximum (FWHM) of the A_1 chalcopyrite band has been suggested as an appropriate parameter for such purpose. Since the inverse of the FWHM of a Raman band is essentially a measurement of the phonon lifetime (convoluted with the transfer function of the optical system), the presence of any type of crystalline defects contributes to enhancing the probability of phonon scattering, thus resulting in a broadening of the Raman bands.

In the case of CIS and CISe photovoltaic absorbers, it is well established that the increase of the FWHM of the A_1 band correlates with a worsening of the film crystallinity, as inferred from Transmission Electron Microscopy (TEM), Scanning Electron Microscopy (SEM) and X-Ray Diffraction (XRD) observations.[8,9] Furthermore, the significance of the absorber crystalline quality has been revealed by several studies that have reported good correlations between the FWHM of the A_1 band and the electrical performance of the corresponding solar cells. In particular, Open Circuit Voltage (V_{OC}) and cell efficiency (η) have both shown[10–12] to be strongly dependent on the FWHM of the A_1 band. Even though the relationship between FWHM and the electrical parameters is not necessarily linear, it is still possible to use this parameter to define a window for the production process by defining a maximum acceptable FWHM, below which the expected device efficiency would not be compromised by the quality of the absorber.

Fig. 2 shows the correlation observed from the analysis of the electrodeposited S-rich $CuIn(S,Se)_2$ absorbers.[12] This experimental relation allowed defining a threshold value for the FWHM, in order to reject absorbers yielding cells with efficiencies below 8.5%. In spite of the validity of these correlations, it should be kept in mind that the electrical performance of the solar cells may be conditioned by other parameters not directly related to the absorber properties. Therefore, RS should be regarded as a monitoring tool for ensuring a certain crystalline quality of the absorber, but cannot obviously grant the validity of all the steps involved in the production of a photovoltaic device.

The presence of a high density of point or extended defects—such as dislocations, twins or grain boundaries in nanocrystalline layers—also determines a change in the shape of the A_1 band, with an asymmetric broadening and shift towards higher wavenumbers, because of the activation of higher frequency phonons with a non-zero wave vector.[9,10]

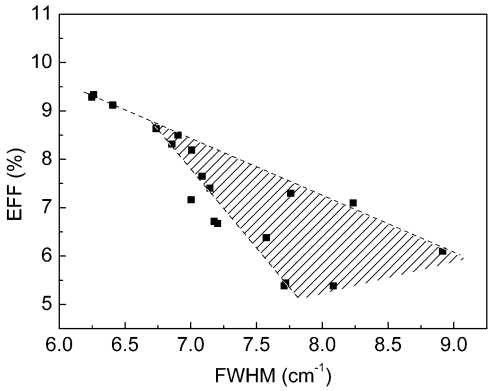

Fig. 2 Efficiency *versus* FWHM of A_1 CIS mode from electrochemical based S-rich $CuIn(S,Se)_2$ solar cells. Shadowed area corresponds to cells with efficiency lower than 8.5% (corresponding to FWHM higher than 6.8 cm^{-1}).

This results from the relaxation of the momentum conservation law caused by the breakage of the crystalline symmetry. In these cases, the shape of the Raman band can be modelled assuming a correlation length model,[9] and the estimation of the correlation length gives a quantitative estimation of the degree of disorder in the crystals related to the presence of a high density of defects. In the case of nanocrystalline layers, the correlation length may be physically limited by the size of the crystal itself.

Identification of structural polytypes. The chalcopyrite structure is the most thermodynamically stable crystalline phase of CIS, CISe, CGS, and CGSe at 0 K. However, at higher temperatures, the formation of other structural polytypes becomes favourable, particularly in the case of CIS and CISe materials.[13] At common temperatures occurring during film formation, the Cu–Au polytype ($P\bar{4}m2$) becomes a nearly isoenthalpic structure with respect to the chalcopyrite equilibrium phase. This polytype is labelled as "Cu–Au" because of the analogy of the cationic distribution in this crystal structure, in which cations form alternative planes of Cu and In, in such a way that they resemble the structure of the copper–gold alloy. The formation energy of this polytype in CIS and CISe is only of about 2 meV per atom, even at room temperature. As a result, formation of metastable Cu–Au ordered domains in CIS and CISe absorbers may occur, depending on the processing conditions. In particular, it has been observed that Cu–Au ordering is favoured in CIS films by Cu poor growth conditions, as well as by low temperature processes.[14]

Since variations in the crystallographic structure lead to a different spectrum of phonon frequencies, the presence of Cu–Au ordered CIS and CISe can be both readily detected by means of RS. The most distinctive feature of this phase in the Raman spectrum is a band corresponding to an A_1 vibrational mode that appears at about 305 cm^{-1} (Cu–Au CIS) and 183 cm^{-1} (Cu–Au CISe), respectively.[15]

Fig. 3 shows the Raman spectrum from a CIS layer grown under conditions favouring the coexistence of both Cu–Au ordered and chalcopyrite phases. In terms of process monitoring, the identification of the formation of Cu–Au polytypes is of

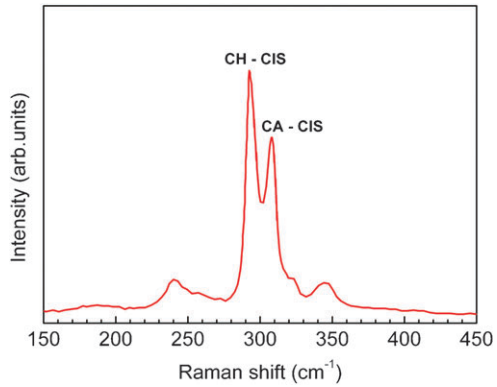

Fig. 3 Raman spectrum from a CIS layer showing the main modes characteristic of Cu–Au and chalcopyrite ordered polytypes.

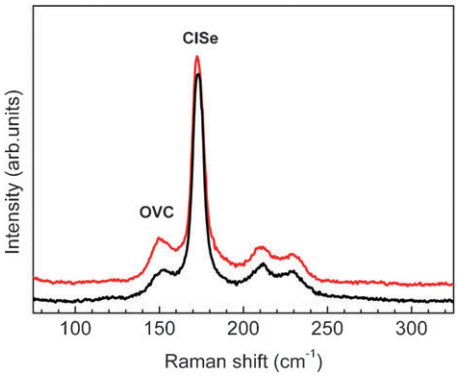

Fig. 4 Raman spectra from Cu-poor $CuInSe_2$ layers (up: Cu/In $\approx$ 0.66, low: Cu/In $\approx$ 0.71), showing the OVC main contribution at the 150–160 cm^{-1} region, in addition to the A_1 CISe mode. Spectra are normalised to the intensity of the A_1 CISe peak, and spectra from the different samples are vertically shifted.

great importance, since in general, their formation is associated with a degradation of the quality of the absorber, and with a poor photovoltaic performance. However, the detection of these structures is not always straightforward by means of other techniques, including XRD, due to the fact that these polytypes often appear as nanometric size domains. Even in these cases, RS has proved itself as an extremely sensitive method to investigate the structural properties of these films.

Identification of secondary phases. Several secondary phases may form during the synthesis of chalcopyrite absorbers. In some cases, these phases have a positive effect in the characteristics of the final device. However, in general their presence in the absorbers has a detrimental effect and is totally undesirable. This is the case of CuSe binaries in CISe, or CuS binaries and the spinnel type $CuIn_5S_8$ in CIS.

During the synthesis of CIS based absorbers, formation of Cu(S,Se) phases at the surface region of the layers is favoured by the use of Cu excess conditions that allow the formation of layers with improved crystalline quality.[14] The presence of these phases can be easily detected from their characteristic fingerprint bands.[16] Since these phases are commonly removed by means of a chemical etching process (as will be shown in Fig. 7), RS can be used also to ensure the effectiveness of this step.

Another remarkable case is the identification of Ordered Vacancy Compounds (OVCs) in CISe based absorbers. These phases arise as a result of a deficiency of Cu during the film formation, leading to the introduction of randomly distributed In_{Cu} antisite defects in the chalcopyrite lattice, which are electrically compensated by Se vacancies. Several OVCs with different stoichiometries have been reported in the literature, including $CuIn_2Se_{3.5}$, $CuIn_3Se_5$, and $CuIn_5Se_8$.[17] CISe absorbers are typically grown with a Cu content below the stoichiometry of $CuInSe_2$, in order to avoid the presence of CuSe binaries that, in this case, are formed inside the layers.[18] This leads to the formation of an OVC phase at the surface region of the layers that has been reported to have a beneficial effect on the characteristics of the cells because of band bending and alignment. Identification and characterisation of OVCs by RS can be performed through its characteristic A_1(OVC) band. The frequency of this band is related to the chemical composition of the OVC phase. The introduction of vacancies results in an effective weakening of the cation–anion bond, thus shifting the A_1 band towards lower frequencies with respect to the reference position in the chalcopyrite lattice. This can be seen in Fig. 4, which shows the Raman spectra measured from Cu-poor $CuInSe_2$ layers grown with a co-evaporation process as described in ref. 19. Furthermore, the relative intensity of the A_1(OVC) band can be used as an estimator of the relative content of this phase, with respect to the chalcopyrite phase.

In addition to the potential of RS for monitoring of the film surface, it should be pointed out that this technique also allows investigating the interfaces of the films, by using the micro-Raman configuration in cross-section measurements. This procedure allows us to identify the formation of MoS_2 and $MoSe_2$ at the back contact interface.[20,21] The presence of such interfacial phases has a relevant effect on the characteristics of the devices, as they prevent from the formation of a Schottky barrier at the back region of the cell. On the other hand, they might be also responsible in some cases for film adhesion failure.[22,23]

Characterisation of quaternary chalcopyrite alloys. Exploitation of the potential of chalcopyrite based materials for high efficiency solar cells requires for the use of quaternary alloys, which allows adjusting the optoelectronic properties of the film to those required for optimal devices. In fact, the best efficiency results have been obtained up to now with the aid of Ga and S alloying, and using CISe as the base material. The strong influence that small variations of the composition of the alloys can have on the characteristics of the resulting film rises the interest on the availability of non-destructive monitoring techniques for the quantitative analysis of the degree of alloying.

RS is a suitable method to determine the composition of chalcopyrite quaternary alloys. In the case of CIS–CGS and CISe–CGSe alloys, the introduction of two types of trivalent cations (Ga and In) in the lattice results in a composition dependent effective force constant, which shifts the A_1 band from its reference position in the Ga-free ternary, to the one in the In-free crystal. Moreover, since this shift is linear, the determination of the alloy composition is straightforward from the analysis of the frequency of the A_1 band. This can

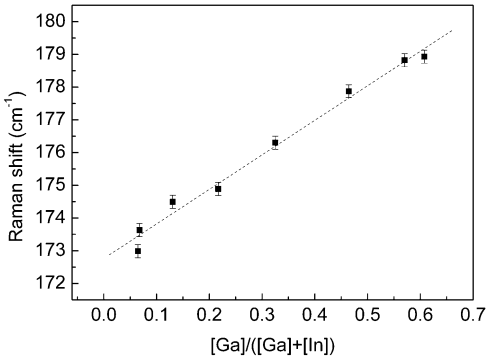

Fig. 5 Frequency of A_1 mode *versus* Ga/(In + Ga) content ratio from $Cu(In_xGa_{1-x})Se_2$ alloys. Dashed line corresponds to the linear fitting of the experimental data.

be seen in Fig. 5, where the frequency of the A_1 mode is plotted *versus* the Ga/(In + Ga) relative content in CISe–CGSe based alloys. Combination of these measurements with an etching procedure allows for the in-depth resolved analysis of the composition of the alloy. This is especially useful for the characterisation of inhomogeneous layers with gradual composition that are developed for higher efficiency devices.[6]

In the case of anion alloying, the interpretation of the Raman spectrum is slightly more complex. However, it is still possible to quantitatively establish the degree of S–Se alloying. The A_1 chalcopyrite band in these alloys presents a two-mode behaviour, characterised by the presence of two modes corresponding to S–S and Se–Se vibrations, being the position and relative intensity of the Se–Se band sensitive to composition variations in the alloy.[2,24]

On the other hand, a significant increase in the sensitivity of RS to changes in the alloy composition can be obtained by the use of measurements obtained at quasi-resonant conditions. Quasi-resonant measurements can be achieved by selecting an excitation wavelength close enough to the band-gap of the alloy.[25] This determines a strong increase of the intensity of the Raman modes, which allows for a significant decrease of the measuring time.

Quasi-resonant Raman excitation measurements have been successfully applied to the determination of the S/(S + Se) relative content in electrodeposited S-rich CISe–CIS quaternary alloys.[26] In this case, a fixed excitation wavelength of 785 nm was used, while alloys with relative S/(S + Se) content between 70%–100% were analysed. Fig. 6 shows the Raman spectra measured from these layers. These spectra are characterised by the presence of several first order modes located at the 250–350 cm^{-1} spectral region, as well as second order peaks that appear in the 500–700 cm^{-1} spectral region. This contrasts with the spectra measured without resonance, where only the A_1 S–S mode is clearly detected.[2] Increasing the content of Se in the alloy leads to a deviation of the band gap from resonant conditions, and this determines a strong decrease in the intensity of the modes. This is clearly reflected in the inset in the figure, which shows the existence of an exponential dependence of the intensity of the main mode in the spectra with the S content.

These quasi-resonant measurements provide with a fast and non-destructive tool for the detection of deviations in the

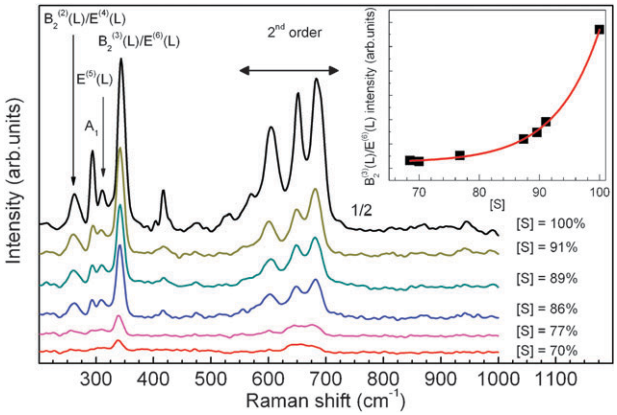

Fig. 6 Quasi-resonant Raman spectra from $CuIn(S,Se)_2$ layers with different composition. Spectra from the different layers are vertically shifted. Inset in the figure shows the dependence of the intensity of the $B_2^{(3)}(L)/E^{(6)}(L)$ mode at about 340 cm^{-1} on the alloy composition. The line in the inset corresponds to the fitting of the data with an exponential law.

composition and band gap of the absorbers. By a suitable selection of the excitation wavelength, the technique can be extended to the investigation of alloys with different composition from the $Cu(In,Ga)(S,Se)_2$ system. Using a suitable microscopic excitation and light collection optics, mapping measurements with high lateral resolution can be achieved, allowing for the analysis of local band gap and composition inhomogeneities that are strongly relevant for the efficiency of the devices.

Raman scattering monitoring of electrodeposition processes in electrodeposited $CuIn(S,Se)_2$ solar cells

This section describes the application of RS for the monitoring of the electrodeposition processes involved in the fabrication of electrochemical based $CuIn(S,Se)_2$ solar cells. Single step electrodeposition of nanocrystalline $CuInSe_2$ precursors followed by a reactive annealing under sulfurising conditions leads to the formation of high crystalline quality absorbers, obtaining solar cell efficiencies up to 11%.[4] Further development of these processes has a strong interest because of their potential to achieve a significant reduction of production costs in relation to standard industrial technologies that are based on the use of Physical Vapour Deposition processes.

Fig. 7 shows a schematic representation of the main steps involved in the fabrication of electrochemical based solar cells that can be potentially assessed by RS. These include: (i) assessment of chemical composition and the presence of secondary phases in electrodeposited precursors;[27,28] (ii) characterisation of sulfurised layers (degree of sulfurisation and crystalline quality of absorber layers);[8,26] (iii) monitoring of NaCN etching (removal of Cu-rich surface secondary phases);[16] and (iv) analysis of thickness of CdS buffer layer.[29]

In relation to these steps, special emphasis is given to the assessment of the electrodeposition process, because of the strong influence of the characteristics of the $CuInSe_2$ precursors on the optoelectronic properties of the sulfurised absorbers. RS analysis of the electrodeposited precursors has allowed identification of the main secondary phases in the layers with

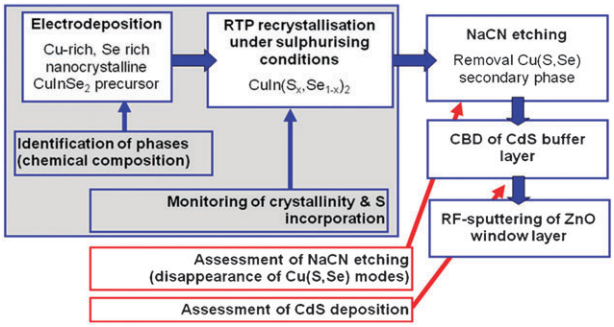

Fig. 7 Schematic representation of the processes involved in the fabrication of electrochemical based S-rich CuIn(S,Se)2 solar cells, indicating the main steps that can be monitored by Raman scattering. Grey box indicates the processes that are involved in the synthesis of the absorbers.

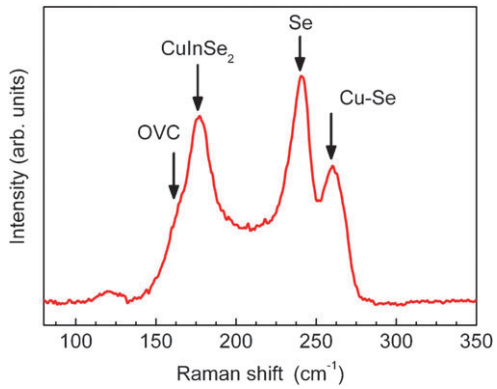

Fig. 8 Raman spectrum from an electrodeposited $CuInSe_2$ precursor with $m = 1.7$, showing the spectral contributions characteristic of the different phases present in the layer.

elemental Se,[30] Cu–Se binary compounds and OVC phases, as shown in Fig. 8.[27,28] The characterisation of precursors grown under conditions leading to different values of stoichiometry (m = 2Se/(Cu + 3In)) reveals the existence of a strong dependence of the relative intensity of both elemental Se and Cu–Se modes on the layer composition, being the formation of these phases controlled by the Se excess in the layers. On the other hand, the composition of the precursors has a strong impact on the characteristics of the final solar cells, which leads to the existence of an optimum range of values of stoichiometry m for the electrodeposited precursors in terms of the solar cell efficiency. All these give a strong interest to the monitoring and control of the composition of the precursors at the electrodeposition step.

One of the main problems related to the implementation of Raman scattering for the on-line and *in situ* monitoring of the electrodeposition processes is due to the existence of a strong background signal from the aqueous electrolyte that hinders the direct observation of the modes from the precursor layer immersed in the electrolytic bath. This can be seen in Fig. 9 (left), where the spectra measured with the probe immersed in the electrolyte with and without a precursor layer in the cell are plotted.

This can be solved by using a differential procedure, where the spectrum measured with the sample immersed in the

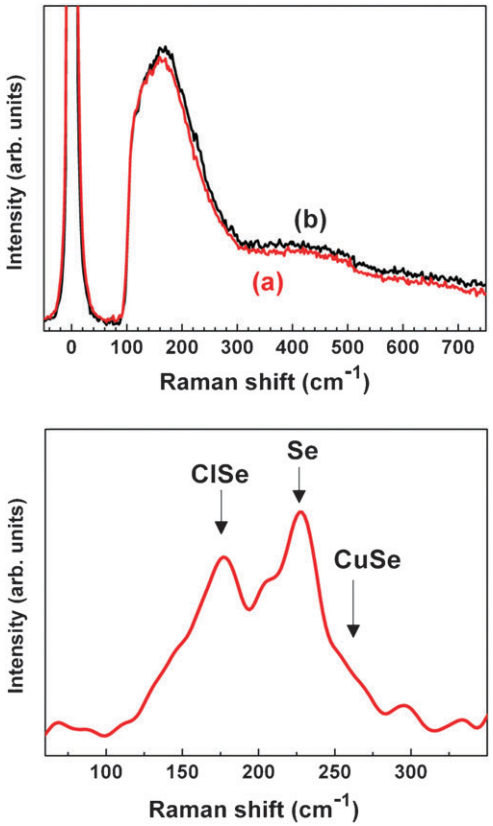

Fig. 9 Left: Raman spectra from the electrolytic bath (a) and the $CuInSe_2$ electrodeposited precursor with $m = 1.52$ immersed in the bath (b). Right: Raman spectrum from the precursor layer after subtracting from the background signal and noise filtering.

electrolyte is subtracted from the spectrum measured without any sample in the electrolytic cell. As shown in Fig. 9 (right), even though the resulting spectra are obviously affected by the background, most of the characteristic Raman bands are still recognisable, which probes the potential of these measurements for the detection at on-line/*in situ* conditions of the presence of the different phases in the precursor layers.

For the systematic analysis of these measurements, a procedure has been developed that is based on the analysis of the integral intensity of the experimental spectra at the regions where the contributions from the different phases appear.[31] Fig. 10 shows the plot of the relative intensity of the bands corresponding to the Se-rich modes and the OVC contribution in relation to that of the main $CuInSe_2$ phase from the measurements performed at on-line conditions (with the layer still at the electrochemical cell). Typical measuring times of these spectra are of 1–10 s. As shown in the figure, and in spite of the relatively high level of noise of these measurements and the simplicity of their processing, the experimental data show a clear correlation with the stoichiometry of the layers. In both cases, it is possible to obtain an accurate fitting of the data with simple linear relationships. This gives a simple experimental procedure for the early detection of deviations in the composition of the precursors from the optimum range of values previously defined for the used electrodeposition conditions (shown in the figure).

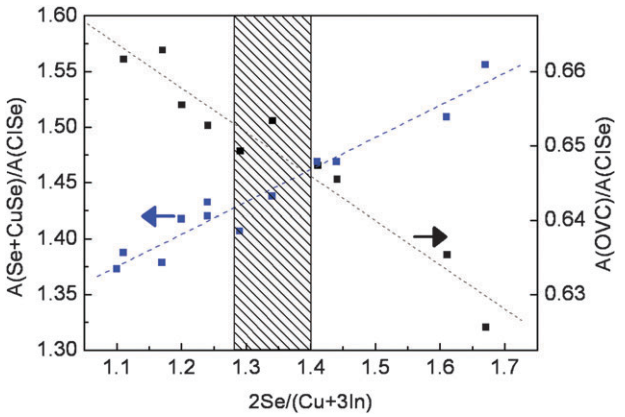

Fig. 10 Relative integral intensity of spectral contributions corresponding to Se rich (Se + (Cu–Se)) and OVC phases in relation to that from the main CISe phase in the electrodeposited precursors, *versus* layer stoichiometry. Dashed lines correspond to the linear fitting of the experimental data. The vertical bar in the figure indicates the optimum range of values of stoichiometry of the precursors for the selected process conditions.[27]

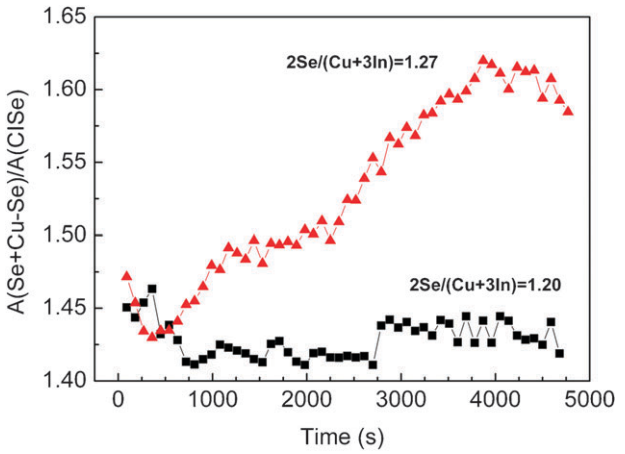

Fig. 11 Real time evolution of the relative integral intensity of the spectral contributions corresponding to Se rich (Se + (Cu–Se)) phases in relation to that from the main CISe phase during the electrochemical growth of the $CuInSe_2$ precursors, for processes leading to layers with different stoichiometry values.

On the other hand, the short measuring time required for these measurements allows also for their implementation at *in situ* real time conditions. Fig. 11 shows the time evolution of the relative intensity at the spectral region corresponding to the Se-rich modes in relation to that of the main $CuInSe_2$ phase during the electrochemical growth of the layers, for electrodeposition conditions corresponding to two different stoichiometry values of the grown layers. As shown in the figure, differences in the process parameters lead to strong differences in the time evolution of this signal. This opens the possibility for the use of these measurements for the monitoring of the process at real time conditions, by comparing the evolution of the measured data with that obtained from standard calibrated processes at well defined conditions. Feedback of these data to the process parameters would allow for the development of active control procedures during the electrodeposition process.

Conclusions

In this work the development of Raman scattering based strategies for process monitoring in chalcopyrite based photovoltaic thin film technologies is reported. Raman spectra measured at different process steps during the fabrication of the absorbers are very sensitive to features related to their crystalline quality, the presence of secondary phases and polytypes and alloy composition. All these are features that have a significant impact on the characteristics of the final solar cells. New strategies based on the use of quasi-resonant Raman measurements are described for the non-destructive assessment of the composition of quaternary alloys. The implementation of Raman scattering for monitoring of electrodeposition processes used in the fabrication of low cost electrochemical based $CuIn(S,Se)_2$ solar cells is reported at both on-line and *in situ* levels. The results obtained corroborate the potential of Raman scattering based techniques for process monitoring applications, either as an "on-line" or "*in situ*" quality control tool or as a means to monitor the synthesis process of the absorbers chalcopyrite layers.

Acknowledgements

The authors from IREC and University of Barcelona belong to the M-2E (Electronic Materials for Energy) Consolidated Research Group and the XaRMAE Network of Excellence on Materials for Energy of the "Generalitat de Catalunya". This work was partly funded by the LARCIS project (Grant No. SES6-CT-2005-019757) from 6th FP of the European Union, and project ref. FR2009-0014 from the French–Spanish Picasso Cooperative Programme. E. Saucedo also thanks the Spanish Ministry of Science and Innovation for the Juan de la Cierva fellowship.

References

1 M. Powalla, P. Jackson, E. Lotter, D. Hariskos, S. Paetel, R. Würz, R. Menner, W. Wischmann, Presented at the Symp. M (Thin Film Chalcogenide Photovoltaic Materials) of the 2010 E-MRS Spring Meeting (Strasbourg, France, June 2010).
2 R. Scheer, A. Pérez-Rodríguez and W. K. Metzger, *Prog. Photovolt: Res. Appl.*, 2010, **18**, 467–480.
3 J. F. Guillemoles, P. Cowache, S. Massaccesi, L. Thouin, S. Sanchez, D. Lincot and J. Vedel, *Adv. Mater.*, 1994, **6**, 379–381.
4 D. Lincot, J. F. Guillemoles, S. Taunier, D. Guimard, J. Sicx-Kurdi, A. Chaumont, O. Roussel, O. Ramdani, C. Hubert, J. P. Fauvarque, N. Bodereau, L. Parissi, P. Panheleux, P. Fanouillere, N. Naghavi, P. P. Grand, M. Benfarah, P. Mogensen and O. Kerrec, *Sol. Energy*, 2004, **77**, 725–737.
5 R. Caballero, V. Izquierdo-Roca, X. Fontané, C. A. Kauffmann, J. Álvarez-García, A. Eicke, L. Calvo-Barrio, A. Pérez-Rodríguez, H. W. Schock and J. R. Morante, *Acta Mater.*, 2010, **58**, 3468–3476.
6 X. Fontané, V. Izquierdo-Roca, L. Calvo-Barrio, A. Pérez-Rodríguez, J. R. Morante, D. Guettler, A. Eicke and A. N. Tiwari, *Appl. Phys. Lett.*, 2009, **95**, 261912-1.
7 W. H. Koschel and M. Bettini, *Phys. Status Solidi B*, 1975, **72**, 729–736.
8 V. Izquierdo-Roca, A. Pérez-Rodríguez, J. R. Morante, J. Álvarez-García, L. Calvo-Barrio, V. Bermudez, P. P. Grand, L. Parissi, C. Broussillon and O. Kerrec, *J. Appl. Phys.*, 2008, **103**, 123109.
9 C. Camus, E. Rudigier, D. Abou-Ras, N. A. Allsop, T. Unold, Y. Tomm, S. Schorr, S. E. Gledhill, T. Köhler, J. Klaer,

M. C. Lux-Steiner and Ch.-H. Fischer, *Appl. Phys. Lett*., 2008, **92**, 101922.
10 E. Rudigier, T. Enzenhofer and R. Scheer, *Thin Solid Films*, 2005, **480–481**, 327–331.
11 E. Rudigier, J. Álvarez-García, I. Luck, J. Klaer and R. Scheer, *J. Phys. Chem. Solids*, 2003, **64**, 1977–1981.
12 V. Izquierdo, A. Pérez-Rodríguez, L. Calvo-Barrio, J. Álvarez-García, J. R. Morante, V. Bermudez, O. Ramdani, J. Kurdi, P. P. Grand, L. Parissi and O. Kerrec, *Thin Solid Films*, 2008, **516**, 7021–7025.
13 S.-H. Wei, S. B. Zhang and A. Zunger, *Phys. Rev. B: Condens. Matter*, 1999, **59**, R2478.
14 J. Álvarez-García, A. Pérez-Rodríguez, A. Romano-Rodríguez, J. R. Morante, L. Calvo-Barrio, R. Scheer and R. Klenk, *J. Vac. Sci, Technol., A*, 2001, **19**, 232–239.
15 J. Álvarez-García, B. Barcones, A. Pérez-Rodríguez, A. Romano-Rodríguez, J. R. Morante, A. Janotti, S.-H. Wei and R. Scheer, *Phys. Rev. B: Condens. Matter Mater. Phys*., 2005, **71**, 54303-1.
16 V. Izquierdo, A. Pérez-Rodríguez, A. Romano-Rodríguez, J. R. Morante, J. Álvarez-García, L. Calvo-Barrio, V. Bermudez, P. P. Grand, O. Ramdani, L. Parissi and O. Kerrec, *J. Appl. Phys*., 2007, **101**, 103517-1.
17 Ch. M. Xu, X. L. Xu, J. Xu, X. J. Yang, J. Zuo, N. Kong, W. H. Huang and H. T. Liu, *Semicond. Sci. Technol*., 2004, **19**, 1201–1206.
18 A. Virtuani, E. Lotter, M. Powalla, U. Rau, J. H. Werner and M. Acciarri, *J. Appl. Phys*., 2006, **99**, 014906.
19 X. Fontané, V. Izquierdo-Roca, L. Calvo-Barrio, J. Álvarez-Garcia, A. Pérez-Rodríguez, J. R. Morante and W. Witte, *Appl. Phys. Lett*., 2009, **95**, 121907.
20 R. Takei, H. Tanino, S. Chichibu and H. Nakanishi, *J. Appl. Phys*., 1996, **79**, 2793–2795.
21 V. Izquierdo-Roca, X. Fontané, L. Calvo-Barrio, A. Pérez-Rodríguez, J. R. Morante, J. Álvarez-García, F. Duault, L. Parissi and V. Bermúdez, *Thin Solid Films*, 2009, **517**, 2264–2267.
22 N. Kohara, S. Nishiwaki, Y. Hashimoto, T. Negami and T. Wada, *Sol. Energy Mater. Sol. Cells*, 2001, **67**, 209–215.
23 D. Abou-Ras, G. Kostorz, D. Bremaud, M. Kälin, F. V. Kurdesau, A. N. Tiwari and M. Döbeli, *Thin Solid Films*, 2005, **480–481**, 433–438.
24 R. Bacewicz, W. Gebicki and J. Filipowicz, *J. Phys.: Condens. Matter*, 1994, **6**, L777–L780.
25 K. Wakita, H. Hirooka, S. Yasuda, F. Fujita and N. Yamamoto, *J. Appl. Phys*., 1998, **83**, 443–447.
26 V. Izquierdo-Roca, A. Shavel, E. Saucedo, J. S. Jaime-Ferrer, A. Cabot, A. Pérez-Rodríguez, V. Bermudez, J. R. Morante, Presented at the Photovoltaic Technical Conference Thin Film 2010 (Aix-en-Provence, France, May 2010).
27 V. Izquierdo-Roca, X. Fontané, J. Álvarez-García, L. Calvo-Barrio, A. Pérez-Rodríguez, J. R. Morante, J. S. Jaime-Ferrer, E. Saucedo, P. P. Grand and V. Bermúdez, *Thin Solid Films*, 2009, **517**, 2163–2166.
28 O. Ramdani, J. F. Guillemoles, D. Lincot, P. P. Grand, E. Chassaing, O. Kerrec and E. Rzepka, *Thin Solid Films*, 2007, **515**, 5909–5912.
29 J. Palm, W. Stetter, S. Visbeck, T. Niesen, M. Fürfanger, H. Vogt, J. Baumbach, H. Calwer, V. Probst, F. Karg, Proceedings of the 20th European Photovoltaic Solar Energy Conf. (Barcelona, Spain, June 2005), 1699.
30 V. V. Poborchi, A. V. Kolobov and K. Tanaka, *Appl. Phys. Lett*., 1998, **72**, 1167.
31 V. Izquierdo-Roca, E. Saucedo, J. S. Jaime-Ferrer, X. Fontané, A. Perez-Rodriguez, V. Bermudez, J. R. Morante, Presented at the 35th IEEE Photovoltaics Specialists Conference (Hawaii, USA, June 2010).

